ACS OMEGA

Open Access

http://pubs.acs.org/journal/acsodf

Article

Trace Analysis of C_4F_7N Insulating Gas Mixtures by Spontaneous Raman Spectroscopy and Gas Chromatography

Jaspreet Singh,[§] Dawson Dodd,[§] Theresa Evans-Nguyen,[*] and Andreas Muller[*]

Cite This: *ACS Omega* 2024, 9, 20350−20358

Read Online

ACCESS | Metrics & More | Article Recommendations

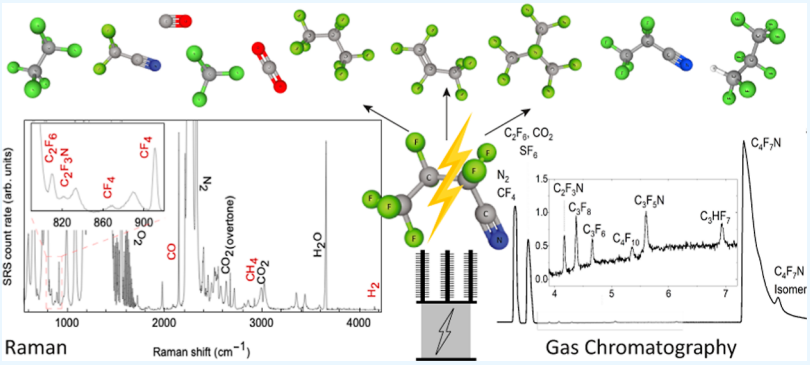

ABSTRACT: 2,3,3,3-Tetrafluoro-2-(trifluoromethyl) propanenitrile (C_4F_7N) is being researched as an alternative to sulfur hexafluoride (SF_6) for applications in gas-insulated switchgear. We independently assessed the effectiveness of gas chromatography−mass spectrometry (GC−MS) and a novel method of feedback-assisted multipass cavity spontaneous Raman spectroscopy (SRS) for the trace quantification of impurities in C_4F_7N and its related byproducts. A total of 14 gases were identified with estimated concentrations as low as 20 ppm (ppm) for C_3F_6 using GC−MS and 7.4 ppm for CH_4 using SRS and as high as 500 ppm for CF_4 using GC−MS and 1430 ppm for CO using SRS. While GC−MS is highly effective in selectively detecting and quantifying trace contaminants, it necessitates separate detectors for various gases, such as CH_4 and H_2. SRS succeeded in detecting CF_4 and C_2F_6 at concentrations of 465 and 100 ppm, respectively, and in placing an upper bound of several hundred ppm for the other analytes. Crucially, SRS holds potential for portability—and thus for field applications—in gas-insulated switchgear equipment diagnostics.

INTRODUCTION

Sulfur hexafluoride (SF_6) is among the most popular insulating gases and is employed in a variety of industries. Its most common application is as an arc quenching gas in high-voltage electrical switchgear systems due to its optimal dielectric properties and very stable nature derived from its octahedral geometry.[1−4] However, SF_6 is categorized as a highly potent greenhouse gas with a global warming potential (GWP) of 23,500.[5−7] SF_6 is now reported to have an atmospheric lifespan of 850 years, with electron attachment identified as the primary removal process, although a lifespan of 3200 years and UV radiation-triggered photolysis as the main removal mechanism were previously reported by the Intergovernmental Panel on Climate Change (IPCC).[8,9] There is thus a need for an appropriate replacement gas that has properties similar to those of SF_6 but without the environmental impact.

When designing SF_6 alternatives, many properties need to be considered, including dielectric strength, environmental impact, boiling point, interactions with common materials, toxicity, and others.[10−12] A current candidate is 2,3,3,3-tetrafluoro-2-(trifluoromethyl) propanenitrile (C_4F_7N). Its low GWP of 2400 and superior dielectric strength make C_4F_7N a promising alternative.[13−15] However, it has to be mixed with CO_2, O_2, or N_2 to be used industrially due to its −4.7 °C boiling point.[16] When decomposed, C_4F_7N can form many potentially harmful byproducts, including CO, CF_4, C_2F_4, CF_3CN, C_2F_6, C_4F_{10}, C_3F_8, C_3F_6, C_4F_6, and others.[17,18] Consequently, there is high demand for an analytical tool that can perform chemical diagnostics for gas preparation and can monitor trace concentrations during operation/handling/disposal to comply with quality and safety controls.

One of the most common and versatile methods of trace gas detection is gas chromatography (GC) coupled with mass spectrometry (MS). In the past, GC−MS has been employed

Received: January 25, 2024
Revised: March 22, 2024
Accepted: April 10, 2024
Published: April 26, 2024

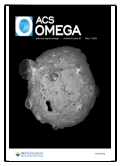

to investigate the decomposition byproducts of C_4F_7N mixtures following discharge, and these findings were corroborated through cross-referencing with various theoretical models, including the reactive molecular dynamics (ReaxFF-MD) method and density functional theory.[19] Li et al. employed a GC−MS system to assess the outcomes of the interaction between a C_4F_7N mixture and the widely utilized gas-insulated equipment sealing material, ethylene propylene diene monomer.[20] A major drawback of GC−MS systems is a bulky footprint associated largely with the need for vacuum operation, which impedes practical applications in the field.

Due to their compact size, nanomaterial-based metal oxide sensors have been investigated as an alternative to GC systems for on-site detection of C_4F_7N. These sensors exhibit an impressive response in the presence of the gas and demonstrate excellent chemical stability.[21,22] Wu et al. used a SnO_2 nanoparticle-based chemiresistive sensor to detect 50 ppm of C_4F_7N with a limit of detection (LOD) of 0.25 parts-per-million (ppm),[23] and, in a later study, 10 ppm of C_4F_7N with LOD of 0.213 ppm.[24] While these sensors exhibit a rapid response time (∼20 s), they are influenced by temperature variations and operate by indirectly detecting gases based on chemically sensitized materials, therefore requiring recurrent calibration.[25]

The optical method of infrared (IR) absorption is a well-established spectroscopic technique for directly analyzing C_4F_7N. Several variants such as Fourier transform infrared spectroscopy (FTIR)[19,26−28] and nondispersive infrared absorption[29] have been extensively investigated as prominent methods for detecting C_4F_7N. While IR spectroscopy offers excellent sensitivity (detection limit ∼ ppm range), a significant challenge it encounters is cross-sensitivity to absorption lines when multiple gases are present simultaneously.[26,30] FTIR resolution can be improved by longer relative path length which however affects portability.[30] Spontaneous Raman spectroscopy (SRS) stands as an alternate optical spectroscopic method for the detection and quantification of trace analytes. As far as our knowledge is concerned, there has been no prior investigation into the utilization of SRS for the detection and measurement of C_4F_7N and its breakdown components. This study aims to assess the potential of SRS in identifying and quantifying both C_4F_7N and its resultant byproducts as a complementary approach to GC−MS, with the potential for field deployment.

BACKGROUND

Fluoronitrile gas mixtures have the potential to strike an optimal balance between dielectric effectiveness and the lowest feasible operating temperature of the equipment, all while significantly diminishing their environmental footprint.[31] Fluoronitriles are typically paired with a buffer gas like N_2, CO_2, or dry air due to their elevated boiling point.[31,32] One such gas is 2,3,3,3-tetrafluoro-2-(trifluoromethyl) propanenitrile, commercially introduced by the 3M company under the trade name NOVEC 4710, with a chemical formula of C_4F_7N; its structure is depicted in Figure 1.

The dielectric strength of C_4F_7N is twice as high as that of pure SF_6, with zero ozone depletion potential.[13,31] Its low GWP is due to the nitrile group reacting with hydroxyl radicals in the air, which decreases its atmospheric lifetime.[12]

The formation of byproducts during the decomposition of C_4F_7N can indeed influence the overall insulation performance of the mixture. However, upon examination of the dielectric

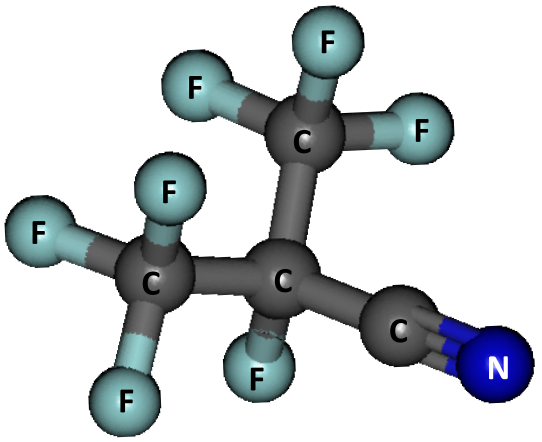

Figure 1. Molecular structure of 2,3,3,3-tetrafluoro-2-(trifluoromethyl) propanenitrile (C_4F_7N). It has C_S symmetry and a σ_h reflection as the only nontrivial symmetry element. The graphic was generated by the Gabedit molecular visualization software.[33]

strength of these individual byproducts through research, it becomes evident that most of them exhibit a dielectric strength either equal to or very close to that of SF_6. Consequently, the insulation capability of the mixture remains largely unaltered after discharges. Furthermore, it is worth noting that the boiling points of these byproducts are similar to or lower than that of C_4F_7N. This implies that none of these byproducts will undergo liquefaction when utilized in appropriate mixtures.[14] Another issue to consider is the toxicity associated with C_4F_7N and its resultant byproducts. Research has indicated that inhaling C_4F_7N can pose a hazard, and furthermore, certain byproducts formed during numerous discharges are known to possess toxic properties. The LC_{50} for C_4F_7N falls within the range of 15,000 to 20,000 ppm, underscoring its potential toxicity when inhaled.[34,35] Byproducts, such as CO, C_2F_6, C_2F_3N, and C_3F_5N, each exhibit an LC_{50} level below 4000 ppm.[35] Given that these byproducts are considerably more toxic than C_4F_7N itself, it is imperative to exercise caution when extracting the gas from switchgear systems. Additionally, it is important to acknowledge their environmental impact. Many of them fall into the category of perfluorocarbons, which are recognized for their detrimental effects on the environment. For instance, C_2F_6 possesses a GWP of 11,000, while CF_4 boasts an atmospheric lifetime of 50,000 years.[7] The formation of these byproducts is affected by multiple factors, such as buffer gas composition, arc current, temperature, circuit breaker geometry, and others.[36] Chen et al. found that C_2F_3N began to form when heated to 500 °C for 72 h.[37] Li et al. discovered that C_4F_7N/N_2 mixtures that use O_2 as an additional buffer gas have an increased CF_4 concentration and a decreased C_2F_6 concentration when discharged.[38] These parameters also affect the insulating ability of C_4F_7N. For example, as the distance between the arc contacts in a circuit breaker increases, the insulating efficiency of the gas is improved.[39] It was also found that the breakdown voltage for mixtures of 20% C_4F_7N and 80% CO_2 follows a nonlinear pattern as pressure increases.[40]

When it comes to general-purpose chemical trace analysis, GC has been the default laboratory technique for separating and analyzing mixtures. Components are separated by moving through a chromatography column before being analyzed by a detector. There are a variety of detectors used in GC that serve

https://doi.org/10.1021/acsomega.4c00846
ACS Omega 2024, 9, 20350−20358

different purposes. For example, electron capture detectors are designed to detect trace amounts of halogen-containing and electronegative compounds very well.[41] When GC is combined with MS, the MS detector can provide mass spectral data, which can be compared to databases for compound confirmation. Here, we employ a quadrupole mass analyzer, which is a nonselective detector commonly used in gas analysis. An important consideration for gas analysis is the type of GC column that is used. Porous layer open tubular (PLOT) columns are a common choice for gas analysis. PLOT columns use solid particles in contrast to a liquid as the stationary phase which does not retain gases as well.[42]

Spontaneous (Stokes) Raman spectroscopy is based on the measurement of the rotational−vibrational spectral fingerprint that gases impart onto monochromatic pump light during inelastic light-matter scattering. SRS trace gas analysis has long been hindered by the relatively small scattering cross sections of order 10^{-31} cm^2/steradian for gases.[43] However, numerous recent efforts into the development of enhancement techniques by way of optical capillaries,[44−46] fibers,[47−53] microcavities,[54] and conventional resonator cavities[55−59] that increase the interaction strength and/or the SRS light collection efficiency have dramatically improved the prospects of SRS for trace gas sensing. Among these enhancement strategies, the utilization of a nonresonant multipass cavity offers particular robustness.[60−66] This technique has demonstrated trace sensitivity well into the parts-per-billion range,[65,66] while requiring minimal power consumption and no active optical resonance stabilization.

The GC−MS system exhibits exceptional sensitivity, capable of detecting gases at exceedingly low concentrations, even in the parts-per-billion (ppb) range. However, despite its remarkable selectivity and low detection thresholds for analytes, its unwieldy size makes it impractical for field deployment. As an on-site leak detection system, GC−MS is not a viable option. Additionally, factors such as instrument cost and operational expenses further hinder the practicality of using the GC−MS system. SRS does not suffer from such limitations. With increasingly cost-effective laser diode sources and array detectors that offer portability, the SRS has emerged as a versatile alternative for gas sensing and quantification.

MATERIALS AND METHODS

All C_4F_7N gas samples, as well as auxiliary calibration gases such as SF_6 and CF_4, were provided by the DILO Company, Inc. The nonmixed C_4F_7N sample was manufactured by 3M (Novec 4710). A sample of C_4F_7N (10%)/CO_2 (85%)/O_2 (5%) that was utilized in a circuit switcher, hereon termed the "discharged sample", was also analyzed. We were not provided with information regarding the process for collecting and retrieving this discharged gas, including details about the site's location and the specific procedures and methods employed. We obtained other gases for analysis, including C_3F_6 (with a purity of 97%), C_4F_{10} (with a purity of 98%), and C_3HF_7 (with a purity of 98%), from Synquest Laboratories Inc.

We utilized a commercial GC−MS instrument with characteristics listed in Table 1. Due to the inability to directly analyze the gases from the cylinders, the samples were extracted and placed into Restek ALTEF gas sampling bags. Subsequently, the gases were extracted from the bags using a gastight syringe and manually injected into the instrument. To perform the analysis, the sample was injected into the inlet of the GC and carried through the column by an inert carrier gas, here, helium. The components of the sample were then separated by interactions with the stationary phase in the column and by the boiling points of the components. Once they exited the column, the components were ionized and traveled through the quadrupole, which allowed ions of certain mass-to-charge ratios to pass through to the detector.

Table 1. Parameters of the GC−MS System

parameter	information
instrument	Agilent 7890B GC/5977B MSD
column	Agilent GS-GasPro 60 m, 0.32 mm ID
carrier gas	helium 1.2 mL/min
ionization	electron impact
split ratio	20:1
oven	120 °C for 20 min
injection volume	20 μL

Figure 2 shows a schematic diagram of the SRS setup. It consists of a multimode blue laser diode (Nichia NUBM44)

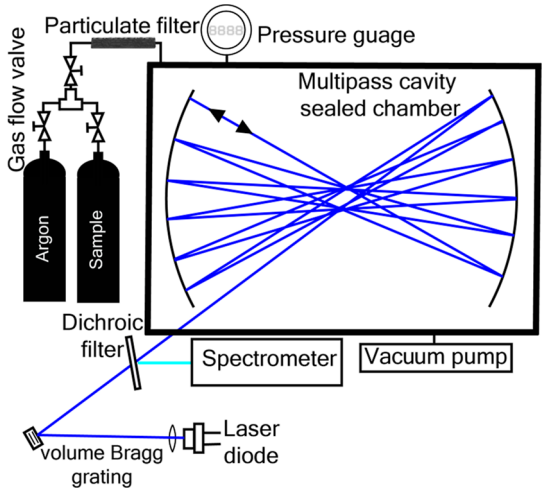

Figure 2. Schematic diagram of the SRS nonresonant, feedback-assisted, multipass cavity chamber in which the various gas samples were analyzed. The chamber incorporates mirrors with a reflectivity greater than 99.99%, such that a large number of passes (∼50) take place. The mirrors form a near-concentric cavity aligned in such a way that the laser beam eventually retraces its path, thereby recycling laser power and enhancing SRS collection. To maintain purity, argon gas purging and backfilling was employed to suppress any residual gases within the chamber.

the emission from which is feedback-coupled via a volume Bragg grating to a retro-reflective multipass cavity. The novel optical characteristics of the setup, in particular a superlinear scaling of the SRS intensity with the number of cavity passes, are explained in prior work.[65] The cavity is located within a sealed chamber into which gases were introduced. Initially, the chamber was depressurized to 0.03 MPa to minimize any remaining background gas. Subsequently, the chamber underwent a series of pumping and purging cycles with argon gas to enhance sample purity within the chamber. Once the chamber was primarily filled with argon and concentrations of any other analytes were sufficiently suppressed, 0.07 MPa of the gas sample was introduced into the chamber from a base pressure of 0.1 MPa. Thus, the chamber, at a total pressure of 1.07 MPa, was filled with the sample at a partial pressure of 0.07 MPa and Ar at a partial pressure of 1 MPa. Spontaneous Raman Stokes

https://doi.org/10.1021/acsomega.4c00846
ACS Omega 2024, 9, 20350−20358

light was collected in a colinear geometry using a dichroic filter and spectrally analyzed with an overall spectral resolution and range of <4 and 500−4200 cm^{-1}, respectively. Excitation and detection polarizations were identical.

RESULTS AND DISCUSSION

Figure 3 shows the outcome of a chromatographic measurement of nominally pure C_4F_7N. The latter compound evidently

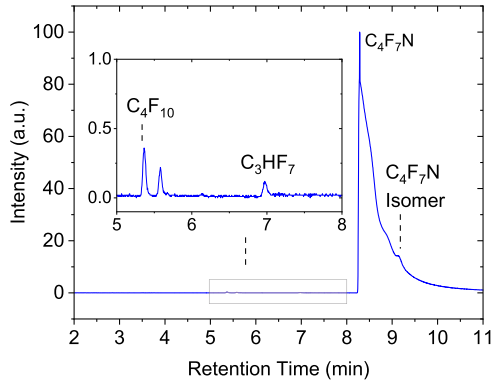

Figure 3. Chromatogram of nominal C_4F_7N. The impurity gases C_4F_{10} and C_3HF_7 could be unambiguously quantified. The gas associated with the unlabeled peak could not be identified.

gives rise to the dominant feature at a retention time of 8.3 min, but close inspection reveals several trace contaminants. This includes an isomer of C_4F_7N, heptafluorobutanenitrile, at a retention time of 9.15 min, an assignment confirmed by a 3M representative. According to 3M, the process used to synthesize C_4F_7N, electrochemical fluorination (ECF), has the potential to introduce small amounts of impurities, including C_4F_{10} and C_3HF_7, both of which were found in our sample. The impurity C_3HF_7 is known to be the most common byproduct during synthesis.[18]

At the retention time of 5.52 min, a peak was present that is associated with a compound that we were not able to identify, as the mass spectrum did not have any good matches in the NIST database. To quantify the impurities in the samples using GC−MS, we created a calibration curve using nominally pure C_3F_6, C_4F_{10}, and C_3HF_7 gases, aided by Agilent MassHunter software. For the nominally pure C_4F_7N sample, we found that the concentration of C_4F_{10} was 50 ppm, and the concentration of C_3HF_7 was 40 ppm. There was no C_3F_6 found in this sample.

The SRS spectrum of nominally pure C_4F_7N gas was acquired at a partial pressure of 0.07 MPa (Figure 4). The primary, dominant SRS peaks were identified at 772 and 2272 cm^{-1}, as seen in the blue trace recorded in 60 accumulated (summed), 1 ms-long measurement (10 ms × 60 exposures). A quantum chemistry simulation using the ORCA software package reveals that these peaks are associated with the symmetric breathing and C−N stretching modes, respectively (red trace in Figure 4).[67] A longer measurement duration consisting of 60, 1 s-long exposures shows numerous other spectral features (green trace of Figure 4).

Given these many C_4F_7N peaks, the detection of trace amounts of impurity gases, such as C_4F_{10} and C_3HF_7, that have SRS peaks in the same range necessitates a minimum concentration to be detectable, that is, a concentration high enough for a characteristic peak to emerge from the background.

To estimate this minimum concentration, we separately acquired SRS spectra of these gases in their pure form under identical pressures and measurement duration. For each gas, a "synthetic" spectrum was then constructed as a sum of the nominal C_4F_7N spectrum and the spectrum of the pure impurity gas scaled down by a known factor. This synthetic spectrum represents the spectrum that would be observed if the impurity were present at the concentration set by the scale factor. Comparing it to the spectrum of C_4F_7N allows us to estimate the minimum impurity concentration as that at which a characteristic peak exceeds the noise levels. For instance, in

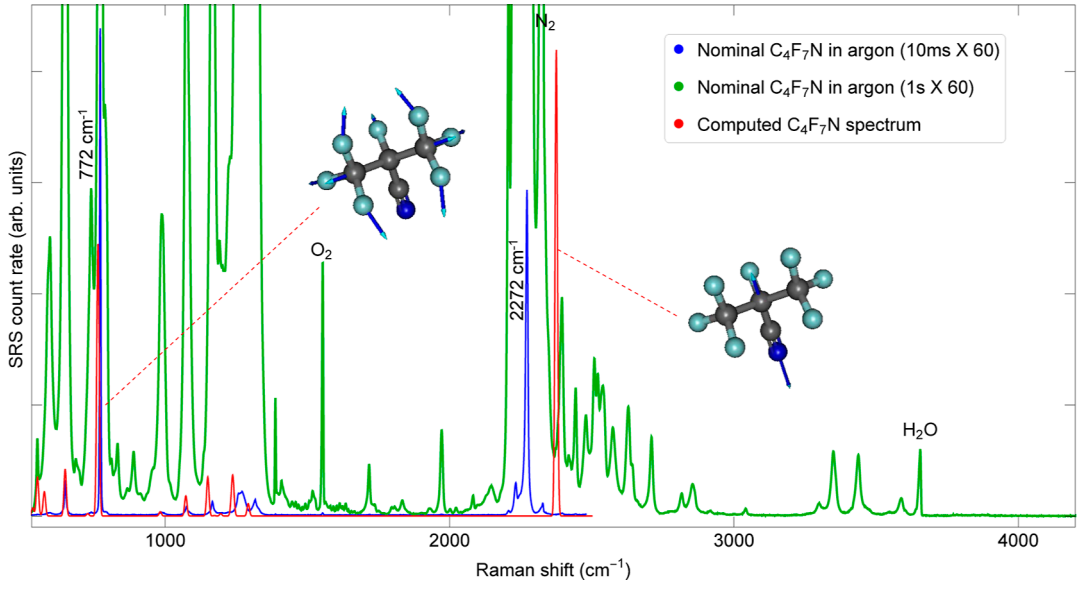

Figure 4. [Two-column] SRS spectrum of nominal C_4F_7N in 10 ms × 60 accumulations (blue) and 1 s × 60 accumulations (green) at a partial pressure of 0.07 MPa. We also plotted the ORCA-generated theoretical Raman spectrum of C_4F_7N (red).[67] Molecular model plots using the Gabedit software show the normal mode displacements associated with the two dominant spectral features.[33]

https://doi.org/10.1021/acsomega.4c00846
ACS Omega 2024, 9, 20350−20358

Figure 5a, upon comparison of the nominal C_4F_7N spectrum with the synthetic spectrum of C_4F_{10} in C_4F_7N, we find that

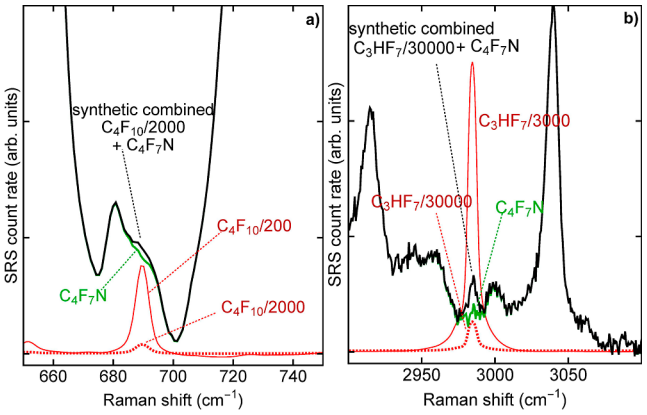

Figure 5. (a) A "synthetic" SRS spectrum (black trace) was constructed as a sum of the nominal C_4F_7N spectrum (green trace) and the spectrum of pure C_4F_{10} gas scaled down by a factor of 2000 (dashed red trace), corresponding to a 490 ppm concentration. For comparison, the spectrum of pure C_4F_{10} gas scaled down by a factor of 200 is also shown (solid red trace). (b) Same as in (a) but for C_3HF_7. All readings were taken at 1 s × 60 accumulations.

when the scale factor is no greater than 2000, which corresponds to a C_4F_{10} impurity concentration of 490 ppm, a characteristic peak at 688 cm^{-1} is visible. Thus, we can conservatively state that the sample contained less than 490 ppm of C_4F_{10}. Similarly, for the case of C_3HF_7 as an impurity, as depicted in Figure 5b, we estimate that a scale factor of no greater than 30,000 reveals a discernible peak at 2984 cm^{-1}, implying the presence of at most 33 ppm of C_3HF_7 in the C_4F_7N sample.

We now turn to the analysis of the discharged $C_4F_7N(10\%)/CO_2(85\%)/O_2(5\%)$ mixture. Using GC−MS and the NIST library, a number of impurities were identified (Figure 6), including CF_4, C_2F_6, SF_6, C_2F_4, C_3F_8, C_2F_3N, C_3F_6, C_4F_{10}, and C_3HF_7. We did not have access to a reference spectrum of C_3F_5N; however, our mass spectrum of the impurity at 5.6 min matches well with the mass spectrum of C_3F_5N obtained by Zhao et al.[14,16−18] In Figure 3, it appears that the unknown peak has the same retention time as C_3F_5N in Figure 6, but when overlapping the spectra, it was found that they indeed have slightly varying retention times. Additionally, the mass spectra of the two peaks do not match. For many of these byproducts, the most abundant fragment is the 69 m/z CF_3^+ fragment, so comparing mass spectra is vital for accurate unambiguous identification. The presence of SF_6 could be due to contaminated tubing being used to fill/empty the circuit switcher, or the C_4F_7N sampling container might have held residual SF_6. In Figure 6a, the N_2 and CO_2 peaks are seen to obstruct the CF_4 and C_2F_6/SF_6 peaks, respectively. In order to distinguish these impurities, we used an extracted ion chromatogram to view only m/z values from 45 to 400 m/z. Since CO_2 and N_2 have m/z values of 44 and 28, respectively, this will allow us to only view values of interest. Using reference standards, we were able to quantify a few of the impurities found in the discharged C_4F_7N (10%)/CO_2 (85%)/O_2 (5%) mixture by creating calibration curves. We found that the concentration of C_4F_{10} was 40 ppm, the concentration of C_3HF_7 was 30 ppm, and the concentration of C_3F_6 was 20 ppm. The remaining impurities were estimated by comparing

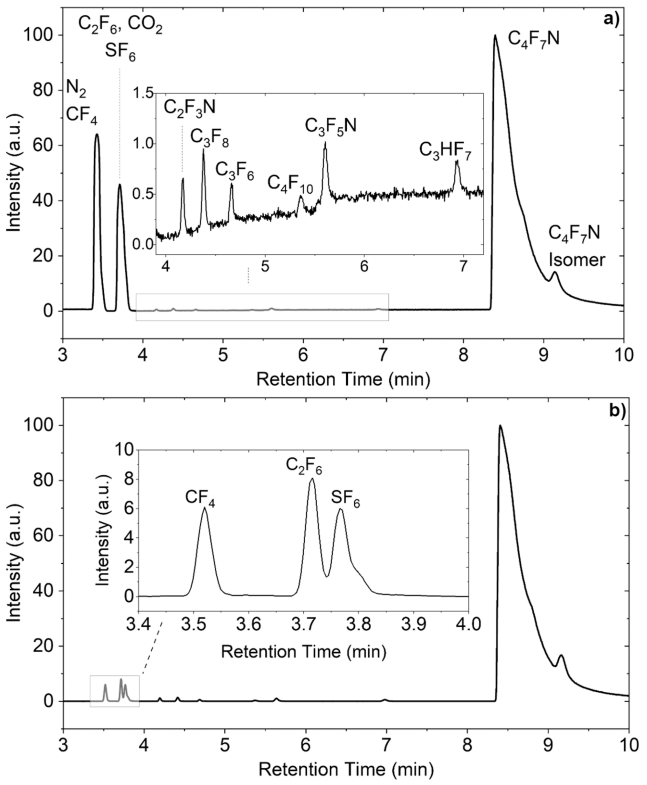

Figure 6. (a) Chromatogram of the discharged $C_4F_7N(10\%)/CO_2(85\%)/O_2(5\%)$ mixture. (b) Chromatogram of the discharged $(10\%)/CO_2(85\%)/O_2(5\%)$ mixture with the contributions of N_2 and CO_2 subtracted.

their different peak areas. These estimated impurities include 500 ppm for CF_4, <120 ppm for C_2F_6, 50 ppm for C_3F_8, 50 ppm for C_2F_3N, 60 ppm for C_3F_5N, and <100 ppm for SF_6.

The SRS spectrum of the discharged C_4F_7N (10%)/CO_2(85%)/O_2(5%) mixture, depicted in Figure 7, was acquired similarly to that of the nominal C_4F_7N sample. The most conspicuous feature, occurring at 2141 cm^{-1}, is associated with carbon monoxide (CO) at a concentration of 1430 ppm. Furthermore, the presence of tetrafluoromethane (CF_4) and hexafluoroethane (C_2F_6) can be attested, with the main peaks at 910 and 810 cm^{-1}, respectively. Their estimated concentrations were 465 and 100 ppm, respectively. The peak at 820 cm^{-1} is assigned to trifluoroacetonitrile (C_2F_3N).[68] However, a pure sample of C_2F_3N was not available for verification and quantification. Those pure gases that were available to us were utilized to estimate concentration upper bounds, as explained above. The comparison of the synthetic spectrum for C_3F_6 in nominal C_4F_7N with the discharged mixture revealed an estimated upper bound of 400 ppm. Similarly, for the other gases, namely, C_4F_{10} and C_3HF_7, which were also originally present in the nominal C_4F_7N, we estimated their concentration upper bounds in the discharged C_4F_7N. Due to the elevated CO_2 concentration in the discharged C_4F_7N mixture, a higher upper bound of approximately 100 ppm was extracted. Conversely, the upper bound concentration of C_4F_{10} decreased to 200 ppm due to the reduced concentration of C_4F_7N in the mixture. Other gases identified comprise SF_6 at under 1300 ppm, C_2F_3N at 34 ppm, methane (CH_4) at 7.4 ppm, and hydrogen (H_2) at 11.6 ppm. Pure forms of other gases such as C_3F_8 and C_3F_5N, which were detected in GC−MS analysis, were not available to us.

https://doi.org/10.1021/acsomega.4c00846
ACS Omega 2024, 9, 20350−20358

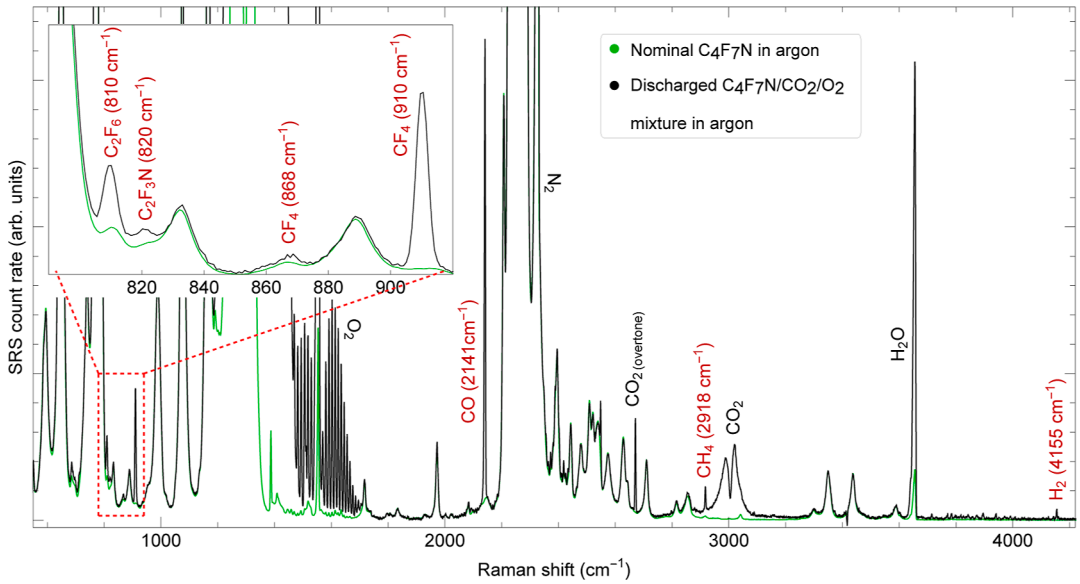

Figure 7. [Two-column] SRS spectrum of the discharged C_4F_7N (10%)/CO_2 (85%)/O_2 (5%) mixture, under 1 s × 60 accumulations at a partial pressure of 0.07 MPa (black trace). In order to facilitate comparison, also represented are the spectrum of the nominal C_4F_7N sample with the same acquisition parameters (green trace), but normalized by the C_4F_7N concentration. Spectral signatures identified, highlighted in red, include those of carbon monoxide (CO) at 2141 cm^{-1}, tetrafluoromethane (CF_4) at 910 cm^{-1}, hexafluoroethane (C_2F_6) at 810 cm^{-1}, trifluoroacetonitrile (C_2F_3N) at 820 cm^{-1}, methane (CH_4) at 2917 cm^{-1}, and hydrogen (H_2) at 4155 cm^{-1}.

Consequently, we did not estimate the detection upper bounds for these gases by SRS.

A summary of the GC−MS and SRS measurements is presented in Table 2. The SRS estimate relies on the Raman differential scattering cross section, $d\sigma/d\Omega$, tabulated for the specific bands indicated by their respective Raman shifts. For some species, such as C_2F_6, this quantity was not available in the literature. As a substitute, the cross section was calculated using the ORCA quantum chemistry software package. We note that the argon purge gas is not included in the determination of the SRS concentrations reported. At the bottom of Table 2 we also report experimental and computed scattering cross sections for two vibrational bands in C_4F_7N.

Table 2. Estimated Concentration of Various Gases Using GC−MS and SRS[a]

gas	common m/z values	GC−MS (ppm)	Raman shift (cm^{-1})	$\frac{d\sigma}{d\Omega}$ rel. to N_2[b]	SRS (ppm)
Gases in Nominal C_4F_7N					
C_4F_{10}	69,119	50 ± 5	688		<490
C_3HF_7	69,151	40 ± 5	2984		<33
Gases in Discharged C_4F_7N(10%)/CO_2(85%)/O_2(5%) Mixture					
CF_4	69,50	500 ± 10	910[69]	1.6[d]	465 ± 100
C_2F_6	69,119	<120	810[70]	2.4[c]	100 ± 10
C_3F_6	69,131	20 ± 5	1794[71]		<388
C_3F_8	69,169	50 ± 10			
C_4F_{10}	69,119	40 ± 5	688		<200
C_3HF_7	69,151	30 ± 5	2984		<100
C_2F_3N	69,76	50 ± 10	820[68]	1.8[c]	34 ± 10
C_3F_5N	69,76	60 ± 10			
SF_6	89,127	<100	1884		<1300
CO			2141[72]	0.9[d]	1430 ± 30
CH_4			2918[73]	7.6[d]	7.4 ± 2
H_2			4155[74]	2.6[d]	11.6 ± 3
C_4F_7N			772	2.2[e]/2.7[c]	
			2272	3.0[e]/4.4[c]	

[a]The bottom entry reports experimental and theoretical Raman cross sections of C_4F_7N. [b]Pump wavelength 443 nm. [c]Calculated using ORCA quantum chemistry software package.[75] [d]Average of cross sections reported in the literature.[72] [e]Experimentally extracted from the C_4F_7N(10%)/CO_2(85%)/O_2(5%) SRS spectrum.

It can be seen in Table 2 that generally speaking there is agreement between the independently obtained concentrations. Additionally, GC−MS and SRS evidently provide complementary capabilities. For example, GC−MS is able to quantify C_3F_8 and C_3F_5N, while SRS is not. Conversely, SRS can quantify C_2F_6, CO, and others that are not quantifiable by GC−MS, at least not with a single detector. Somewhat high discrepancy between GC−MS and SRS was observed, for example, for C_2F_3N, which is however likely attributable to the fact that the SRS cross section was obtained computationally. For many analytes, more precise quantification could be achievable with the availability of calibration samples. For the purpose of safety monitoring, SRS appears to be well suited. For example, carbon monoxide and tetrafluoromethane have been determined to be present in quantities that could present a hazard in an enclosed workspace. In Figure 7, these were recorded in one min, but a much shorter time would suffice to reveal their presence. The SRS analyzer has the advantage of consisting of a single diode laser and array detector, both operating at room temperature and consuming electric power of order of tens of watts at most. Thus, with adequate engineering, a portable device could be constructed with which monitoring could take place directly at switchgear equipment sites.

CONCLUSIONS

With C_4F_7N emerging as an alternative insulating gas to SF_6, so is the need for a comprehensive chemical analysis tool for monitoring gas synthesis and preparation and also discharge gas composition in light of the many potentially harmful byproducts generated. Multipass cavity Raman scattering was

https://doi.org/10.1021/acsomega.4c00846
ACS Omega 2024, 9, 20350−20358

studied in conjunction with GC as a means of rapid chemical analysis. The Raman spectrum of C_4F_7N revealed distinct vibrational bands with sizable scattering cross sections, comparable to those obtained computationally. Samples investigated include nominally pure C_4F_7N and a C_4F_7N-(10%)/CO_2(85%)/O_2(5%) mixture that has been used in switchgear equipment. A number of trace analytes were quantified using both methods. While GC−MS excels at carrying out precise quantification for a wide range of analytes, SRS shows promising attributes such as measurement times of order of a minute, high sensitivity, and high potential for portability.

AUTHOR INFORMATION

Corresponding Authors

Theresa Evans-Nguyen − *Chemistry Department, University of South Florida, Tampa, Florida 33620, United States;* orcid.org/0000-0001-7675-1060; Email: evansnguyen@usf.edu

Andreas Muller − *Physics Department, University of South Florida, Tampa, Florida 33620, United States;* orcid.org/0000-0002-8930-3280; Email: mullera@usf.edu

Authors

Jaspreet Singh − *Physics Department, University of South Florida, Tampa, Florida 33620, United States;* orcid.org/0000-0002-3436-1977

Dawson Dodd − *Chemistry Department, University of South Florida, Tampa, Florida 33620, United States;* orcid.org/0009-0005-9377-4527

Complete contact information is available at: https://pubs.acs.org/10.1021/acsomega.4c00846

Author Contributions

[§]J.S. and D.D. contributed equally.

Notes

The authors declare no competing financial interest.

ACKNOWLEDGMENTS

The authors thank the DILO company for supplying gas samples and acknowledge financial support from the National Science Foundation (NSF grant no. 2116275). We also thank Dr. Laurent Calcul at the USF Chemical Purification Analysis and Screening (CPAS) core facility for his help and for allowing us to use the GC−MS instrument.

REFERENCES

(1) Camilli, G.; Gordon, G. S.; Plump, R. E. Gaseous insulation for high-voltage transformers [includes discussion]. *IEEE Trans. Power Syst.* **1952**, *71*, 348−357.

(2) Li, Y.; Zhang, X.; Zhang, J.; Chen, Q.; Li, Y.; Xiao, S.; Cui, Z.; Tang, J. Thermal compatibility between perfluoroisobutyronitrile-CO_2 gas mixture with copper and aluminum switchgear. *IEEE Access* **2019**, *7*, 19792−19800.

(3) Zhuang, Y.; Hu, X.; Tang, B.; Wang, S.; Cui, A.; Hou, K.; He, Y.; Zhu, L.; Li, W.; Chu, J. Effects of SF_6 decomposition components and concentrations on the discharge faults and insulation defects in GIS equipment. *Sci. Rep.* **2020**, *10*, 15039.

(4) Wang, J.; Wang, P.; Chen, W.; Wan, F.; Lu, Y.; Tang, Z.; Dong, A.; Lei, Z.; Zhang, Z. Highly sensitive multi-pass cavity enhanced Raman spectroscopy with novel polarization filtering for quantitative measurement of SF_6 decomposed components in gas-insulated power equipment. *Sens. Actuators, B* **2023**, *380*, 133350.

(5) Myhre, G.; Shindell, D.; Pongratz, J.. In *Climate Change 2013: The Physical Science Basis; Working Group I Contribution to the Fifth Assessment Report of the Intergovernmental Panel on Climate Change*; Stocker, T., Ed.; Cambridge University Press: Cambridge, 2014; pp 659−740.

(6) Simmonds, P. G.; Rigby, M.; Manning, A. J.; Park, S.; Stanley, K. M.; McCulloch, A.; Henne, S.; Graziosi, F.; Maione, M.; Arduini, J.; et al. The increasing atmospheric burden of the greenhouse gas sulfur hexafluoride (SF_6). *Atmos. Chem. Phys.* **2020**, *20*, 7271−7290.

(7) Xiao, S.; Shi, S.; Li, Y.; Ye, F.; Li, Y.; Tian, S.; Tang, J.; Zhang, X. Review on decomposition characteristics of eco-friendly gas insulating medium for high voltage gas insulated equipment. *J. Phys. D: Appl. Phys.* **2021**, *54*, 373002.

(8) Ray, E. A.; Moore, F. L.; Elkins, J. W.; Rosenlof, K. H.; Laube, J. C.; Röckmann, T.; Marsh, D. R.; Andrews, A. E. Quantification of the SF_6 lifetime based on mesospheric loss measured in the stratospheric polar vortex. *J. Geophys. Res. Atmos.* **2017**, *122*, 4626−4638.

(9) Rabie, M.; Franck, C. M. Assessment of eco-friendly gases for electrical insulation to replace the most potent industrial greenhouse gas SF_6. *Environ. Sci. Technol.* **2018**, *52*, 369−380.

(10) Christophorou, L. G.; Olthoff, J. K.; Green, D. S.; et al. *Gases for Electrical Insulation and Arc Interruption: Possible Present and Future Alternatives to Pure SF_6*; NIST, 1997.

(11) Wang, Y.; Huang, D.; Liu, J.; Zhang, Y.; Zeng, L. Alternative environmentally friendly insulating gases for SF_6. *Processes* **2019**, *7*, 216.

(12) Owens, J.; Xiao, A.; Bonk, J.; DeLorme, M.; Zhang, A. Recent development of two alternative gases to SF_6 for high voltage electrical power applications. *Energies* **2021**, *14*, 5051.

(13) Kieffel, Y.; Biquez, F.; Ponchon, P.; Irwin, T. SF_6 alternative development for high voltage Switchgears. In *2015 IEEE Power & Energy Society General Meeting*, 2015; pp 1−5..

(14) Zhang, B.; Li, C.; Xiong, J.; Zhang, Z.; Li, X.; Deng, Y. Decomposition characteristics of C_4F_7N/CO_2 mixture under AC discharge breakdown. *AIP Adv.* **2019**, *9*, 115212.

(15) Gao, W.; Posada, L.; Shiravand, V.; Shubhashish, S.; Price, C.; Zhang, B.; Potyrailo, R.; Younsi, K.; Shan, S.; Ndiaye, I.; et al. Decomposition characteristics of C_4F_7N-based SF_6-alternative gas mixtures. *J. Appl. Phys.* **2024**, *135*, 063302.

(16) Tang, N.; Chen, L.; Zhang, B.; Li, X. Experimental and theoretical exploration of C_4F_7N gas decomposition under partial discharge. In *2020 IEEE International Conference on High Voltage Engineering and Application (ICHVE)*, 2020; pp 1−4..

(17) Zhao, M.; Han, D.; Zhou, Z.; Zhang, G. Experimental and theoretical analysis on decomposition and by-product formation process of $(CF_3)_2CFCN$ mixture. *AIP Adv.* **2019**, *9*, 105204.

(18) Zhao, M.; Han, D.; Zhao, W.; Zhou, Z.; Zhang, G. Experimental and theoretical studies of C_3F_7CN/CO_2 mixture decomposition under overheating fault. *CSEE J. Power Energy Syst.* **2020**, *8*, 941−951.

(19) Li, Y.; Zhang, X.; Xiao, S.; Chen, Q.; Tang, J.; Chen, D.; Wang, D. Decomposition properties of C_4F_7N/N_2 gas mixture: an environmentally friendly gas to replace SF_6. *Ind. Eng. Chem. Res.* **2018**, *57*, 5173−5182.

(20) Li, Y.; Zhang, X.; Li, Y.; Chen, D.; Cui, Z.; Liu, W.; Tang, J. Interaction mechanism between the $C_4F_7N-CO_2$ gas mixture and the EPDM seal ring. *ACS Omega* **2020**, *5*, 5911−5920.

(21) Jarzebski, Z.; Marton, J. Physical properties of SnO_2 materials: I. Preparation and defect structure. *J. Electrochem. Soc.* **1976**, *123*, 199C−205C.

(22) Batzill, M.; Diebold, U. The surface and materials science of tin oxide. *Prog. Surf. Sci.* **2005**, *79*, 47−154.

(23) Wu, P.; Li, Y.; Xiao, S.; Chen, J.; Tang, J.; Chen, D.; Zhang, X. SnO_2 nanoparticles based highly sensitive gas sensor for detection of C_4F_7N: a new eco-friendly gas insulating medium. *J. Hazard. Mater.* **2022**, *422*, 126882.

(24) Wu, P.; Li, Y.; Xiao, S.; Chen, D.; Chen, J.; Tang, J.; Zhang, X. Room-temperature detection of perfluoroisobutyronitrile with SnO_2/

$Ti_3C_2T_x$ gas sensors. *ACS Appl. Mater. Interfaces* **2022**, *14*, 48200−48211.
(25) Ren, Q.; Cao, Y.-Q.; Arulraj, D.; Liu, C.; Wu, D.; Li, W.-M.; Li, A.-D. Review—resistive-type hydrogen sensors based on zinc oxide nanostructures. *J. Electrochem. Soc.* **2020**, *167*, 067528.
(26) Zhang, Y.; Zhang, X.; Liu, C.; Li, Y.; Cheng, H.; Xiao, H. Research on C_4F_7N gas mixture detection based on infrared spectroscopy. *Sens. Actuators, A* **2019**, *294*, 126−132.
(27) Bian, C.; Dai, F.; Cheng, J.; Tao, J.; Tan, T.; Song, Y. The research on infrared spectrum of C_4F_7N by combined experimental and theoretical study. In *2020 IEEE 4th Conference on Energy Internet and Energy System Integration (EI2)*, 2020; pp 2344−2346..
(28) Liu, W.; Zhao, Y.; Zhang, Y.; Yan, J.; Zhu, Z.; Hu, J. Study on theoretical analysis of C_4F_7N infrared spectra and detection method of mixing ratio of the gas mixture. *J. Mol. Spectrosc.* **2021**, *381*, 111521.
(29) Li, X.; He, S.; Wang, X.; Zeng, X.; Hou, X.; Wu, Q.; Li, J.; Zhu, H. Design and experiment of C_4F_7N/CO_2 mixed gas portable detection system based on NDIR technology. In *Advanced Sensor Systems and Applications X*, 2020; Vol. *11554*; p 1155405..
(30) Zhou, H.-y.; Ma, G.-m.; Wang, Y.; Qin, W.-q.; Jiang, J.; Yan, C.; Li, C.-r. Optical sensing in condition monitoring of gas insulated apparatus: a review. *High Volt.* **2019**, *4*, 259−270.
(31) Nechmi, H. E.; Beroual, A.; Girodet, A.; Vinson, P. Fluoronitriles/CO_2 gas mixture as promising substitute to SF_6 for insulation in high voltage applications. *IEEE Trans. Dielectr. Electr. Insul.* **2016**, *23*, 2587−2593.
(32) Zhang, T.; Zhou, W.; Zheng, Y.; Yu, J. Insulation properties of C_4F_7N/CO_2 mixtures under non-uniform electric field. *IEEE Trans. Dielectr. Electr. Insul.* **2019**, *26*, 1747−1754.
(33) Allouche, A.-R. Gabedit—a graphical user interface for computational chemistry softwares. *J. Comput. Chem.* **2011**, *32*, 174−182.
(34) Tian, S.; Liu, W.; Ding, J.; Liu, J.; Xu, Z.; Yuan, Z.; Zhang, W.; Rao, X.; Wan, Q.; Li, Y.; et al. Study on subacute inhalation toxicity and offspring teratogenicity of C_4F_7N: an environmentally friendly insulating gas to replace SF_6. *J. Clean. Prod.* **2023**, *387*, 135799.
(35) Li, Y.; Zhang, X.; Zhang, J.; Xiao, S.; Xie, B.; Chen, D.; Gao, Y.; Tang, J. Assessment on the toxicity and application risk of C_4F_7N: a new SF_6 alternative gas. *J. Hazard. Mater.* **2019**, *368*, 653−660.
(36) Pietrzak, P.; Perret, M.; Boening, M.; Glomb, S.; Kurte, R.; Franck, C. M. Wear of the arcing contacts and gas under free burning arc in SF_6 alternatives. *IEEE Trans. Power Deliv.* **2023**, *38*, 2133−2140.
(37) Chen, L.; Zhang, B.; Yang, T.; Deng, Y.; Li, X.; Murphy, A. B. Thermal decomposition characteristics and kinetic analysis of C_4F_7N/CO_2 gas mixture. *J. Phys. D: Appl. Phys.* **2020**, *53*, 055502.
(38) Li, Y.; Zhang, X.; Chen, Q.; Zhang, J.; Li, Y.; Xiao, S.; Tang, J. Influence of oxygen on dielectric and decomposition properties of C_4F_7N-N_2-O_2 mixture. *IEEE Trans. Dielectr. Electr. Insul.* **2019**, *26*, 1279−1286.
(39) Pietrzak, P.; Engelbrecht, J. T.; Simka, P.; Janssen, H.; Devaud, P.; Muratovic, M.; Franck, C. M. Voltage−current characteristic of free burning arcs in SF_6 alternative gas mixtures. *IEEE Trans. Plasma Sci.* **2022**, *50*, 4744−4752.
(40) Nechmi, H. E.; Michelarakis, M.; Manu Haddad, A.; Wilson, G. Clarifications on the behavior of alternative gases to SF_6 in divergent electric field distributions under AC voltage. *Energies* **2021**, *14*, 1065.
(41) de Coning, P.; Swinley, J. *A Practical Guide to Gas Analysis by Gas Chromatography*; Elsevier, 2019; pp 247−290.
(42) Wawrzyniak, R. Chapter 5—Gas−solid chromatography (PLOT columns). *Gas Chromatography*; Elsevier, 2012; pp 123−136.
(43) Fenner, W. R.; Hyatt, H. A.; Kellam, J. M.; Porto, S. Raman cross section of some simple gases. *J. Opt. Soc. Am.* **1973**, *63*, 73−77.
(44) Buric, M. P.; Chen, K. P.; Falk, J.; Woodruff, S. D. Multimode metal-lined capillaries for Raman collection and sensing. *J. Opt. Soc. Am. B* **2010**, *27*, 2612−2619.
(45) James, T. M.; Rupp, S.; Telle, H. H. Trace gas and dynamic process monitoring by Raman spectroscopy in metal-coated hollow glass fibres. *Anal. Methods* **2015**, *7*, 2568−2576.
(46) Yu, Y.; Zeng, P.; Yang, C.; Gong, J.; Liang, R.; Ou, Q.; Zhang, S. Gold-nanorod-coated capillaries for the SERS-based detection of Thiram. *ACS Appl. Nano Mater.* **2019**, *2*, 598−606.
(47) Hanf, S.; Keiner, R.; Yan, D.; Popp, J.; Frosch, T. Fiber-enhanced Raman multigas spectroscopy: a versatile tool for environmental gas sensing and breath analysis. *Anal. Chem.* **2014**, *86*, 5278−5285.
(48) Hanf, S.; Bogozi, T.; Keiner, R.; Frosch, T.; Popp, J. Fast and highly sensitive fiber-enhanced Raman spectroscopic monitoring of molecular H_2 and CH_4 for point-of-care diagnosis of malabsorption disorders in exhaled human breath. *Anal. Chem.* **2015**, *87*, 982−988.
(49) Yan, D.; Popp, J.; Pletz, M. W.; Frosch, T. Highly sensitive broadband Raman sensing of antibiotics in step-index hollow-core photonic crystal fibers. *ACS Photonics* **2017**, *4*, 138−145.
(50) Trabold, B. M.; Hupfer, R. J.; Abdolvand, A.; Russell, P. S. J. Broadband high-resolution multi-species CARS in gas-filled hollow-core photonic crystal fiber. *Opt. Lett.* **2017**, *42*, 3283−3286.
(51) Chu, Q.; Jin, Z.; Yu, X.; Li, C.; Zhang, W.; Ji, W.; Lin, B.; Shum, P. P.; Zhang, X.; Wang, G. Volumetric enhancement of Raman scattering for fast detection based on a silver-lined hollow-core fiber. *Opt. Express* **2019**, *27*, 10370−10382.
(52) Beffara, F.; Humbert, G.; Auguste, J.-L.; Perumal, J.; Dinish, U.; Olivo, M. Optimization and performance analysis of SERS-active suspended core photonic crystal fibers. *Opt. Express* **2020**, *28*, 23609−23619.
(53) Qian, G.; Wan, F.; Zhou, F.; Wang, J.; Kong, W.; Chen, W. Fiber-enhanced Raman spectroscopy for trace-gas sensing in the high-concentration gas background with an anti-resonant hollow core fiber. *Front. Phys.* **2022**, *10*, 917688.
(54) Petrak, B.; Djeu, N.; Muller, A. Purcell-enhanced Raman scattering from atmospheric gases in a high-finesse microcavity. *Phys. Rev. A* **2014**, *89*, 023811.
(55) Taylor, D. J.; Glugla, M.; Penzhorn, R.-D. Enhanced Raman sensitivity using an actively stabilized external resonator. *Rev. Sci. Instrum.* **2001**, *72*, 1970−1976.
(56) Salter, R.; Chu, J.; Hippler, M. Cavity-enhanced Raman spectroscopy with optical feedback cw diode lasers for gas phase analysis and spectroscopy. *Analyst* **2012**, *137*, 4669−4676.
(57) Thorstensen, J.; Haugholt, K.; Ferber, A.; Bakke, K.; Tschudi, J. Low-cost resonant cavity Raman gas probe for multi-gas detection. *J. Eur. Opt. Soc., Rapid Publ.* **2014**, *9*, 14054.
(58) Hippler, M. Cavity-enhanced Raman spectroscopy of natural gas with optical feedback cw-diode lasers. *Anal. Chem.* **2015**, *87*, 7803−7809.
(59) Yang, Q. Y.; Tan, Y.; Qu, Z. H.; Sun, Y.; Liu, A. W.; Hu, S. M. Multiple gas detection by cavity-enhanced Raman spectroscopy with sub-ppm sensitivity. *Anal. Chem.* **2023**, *95*, 5652−5660.
(60) Hill, R.; Mulac, A.; Hackett, C. Retroreflecting multipass cell for Raman scattering. *Appl. Opt.* **1977**, *16*, 2004−2006.
(61) Li, X.; Xia, Y.; Zhan, L.; Huang, J. Near-confocal cavity-enhanced Raman spectroscopy for multitrace-gas detection. *Opt. Lett.* **2008**, *33*, 2143−2145.
(62) Petrov, D. V. Multipass optical system for a Raman gas spectrometer. *Appl. Opt.* **2016**, *55*, 9521−9525.
(63) Velez, J. G.; Muller, A. Trace gas sensing using diode-pumped collinearly detected spontaneous Raman scattering enhanced by a multipass cell. *Opt. Lett.* **2020**, *45*, 133−136.
(64) Shen, C.; Wen, C.; Huang, X.; Long, X. A versatile multiple-pass Raman system for industrial trace gas detection. *Sensors* **2021**, *21*, 7173.
(65) Singh, J.; Muller, A. Ambient hydrocarbon detection with an ultra-low-loss cavity Raman analyzer. *Anal. Chem.* **2023**, *95*, 3703−3711.
(66) Singh, J.; Muller, A. High-precision trace hydrogen sensing by multipass Raman scattering. *Sensors* **2023**, *23*, 5171.
(67) Neese, F. The ORCA program system. *Wiley Interdiscip. Rev.: Comput. Mol. Sci.* **2012**, *2*, 73−78.
(68) Gullikson, C.; Nielsen, J. R. Raman spectrum of gaseous trifluoroacetonitrile. *J. Mol. Spectrosc.* **1957**, *1*, 155−157.

https://doi.org/10.1021/acsomega.4c00846
ACS Omega 2024, 9, 20350−20358

(69) Monostori, B.; Weber, A. The Raman spectrum of gaseous CF_4. *J. Chem. Phys.* **1960**, *33*, 1867−1868.
(70) Carney, R. A.; Piotrowski, E. A.; Meister, A. G.; Braun, J. H.; Cleveland, F. F. Substituted ethanes: Part V. Raman and infrared spectra, assignments, potential constants, and calculated thermodynamic properties for C_2F_6, C_2Cl_6, and C_2Br_6. *J. Mol. Spectrosc.* **1961**, *7*, 209−222.
(71) Nielsen, J. R.; Claassen, H.; Smith, D. Infrared and Raman spectra of fluorinated ethylenes. V. Hexafluoropropene. *J. Chem. Phys.* **1952**, *20*, 1916−1919.
(72) Schrötter, H.; Klöckner, H. Chapter Raman scattering cross sections in gases and liquids. In *Raman Spectroscopy of Gases and Liquids*; Weber, A., Ed.; Springer, 1979; pp 123−166.
(73) Magnotti, G.; Kc, U.; Varghese, P.; Barlow, R. Raman spectra of methane, ethylene, ethane, dimethyl ether, formaldehyde and propane for combustion applications. *J. Quant. Spectrosc. Radiat. Transfer* **2015**, *163*, 80−101.
(74) Veirs, D. K.; Rosenblatt, G. M. Raman line positions in molecular hydrogen: H2, HD, HT, D2, DT, and T2. *J. Mol. Spectrosc.* **1987**, *121*, 401−419.
(75) Neugebauer, J.; Reiher, M.; Kind, C.; Hess, B. A. Quantum chemical calculation of vibrational spectra of large molecules—Raman and IR spectra for Buckminsterfullerene. *J. Comput. Chem.* **2002**, *23*, 895−910.

https://doi.org/10.1021/acsomega.4c00846
ACS Omega 2024, 9, 20350−20358